Research Square

Preprints are preliminary reports that have not undergone peer review.
They should not be considered conclusive, used to inform clinical practice,
or referenced by the media as validated information.

In Vivo Antitumor Efficacy of 17-AAG Loaded PMMA in a Multiple Myeloma Patient-Derived Xenograft Mouse Model

Xiangjun Shi
Beijing Chao-Yang Hospital: Beijing Chaoyang Hospital
Yanzhe Wei
Beijing Chao-Yang Hospital: Beijing Chaoyang Hospital
Xingchen Yao
Beijing Chao-Yang Hospital: Beijing Chaoyang Hospital
Boran Du
Capital Medical University Beijing Obstetrics and Gynecology Hospital
Xiaoguang Wu
Chengde Medical University
Xiangyu Kong
Chengde Medical University
Xinru Du (duxinru@ccmu.edu.cn)
Beijing Chao-Yang Hospital: Beijing Chaoyang Hospital https://orcid.org/0000-0002-7282-1997

Research Article

Keywords: Multiple Myeloma, PMMA, 17-AAG, PDX-model, Apoptosis

Posted Date: August 12th, 2021

DOI: https://doi.org/10.21203/rs.3.rs-779284/v1

License: This work is licensed under a Creative Commons Attribution 4.0 International License.
Read Full License

Abstract

Multiple myeloma (MM) is a monoclonal malignancy characterized by abnormal proliferation of plasma cells. Its main clinical symptoms are osteolytic damage, severe bone pain, spinal instability, and pathological fracture and are collectively referred to as multiple myeloma bone disease (MMBD). Due to its good biomechanical properties and fast curing, polymethylmethacrylate (PMMA) bone cement is widely used for bone repair after MMBD surgery. However, whether drug-loading PMMA can inhibit tumor growth and angiogenesis has not been reported. Here, we report that 17-AAG-loaded PMMA bone cement inhibits MM growth *in vivo* and suppresses tumor diffusion to peripheral tissues. 17-AAG-loaded PMMA promotes MM apoptosis by downregulating Bax and active Caspase-3.

Introduction

Multiple myeloma (MM) is the second largest hematologic malignancy, characterized by abnormal monoclonal plasma cell proliferation and high monoclonal immunoglobulin secretion[1,2]. More than 90% of multiple myeloma bone disease (MMBD) is characterized by osteolytic bone destruction and no new bone formation, seriously affecting quality of life [3–5]. The most frequently involved sites are the axial and limb bones [6]. Spinal involvement accounts for more > 20% of primary spinal tumors [7]. Surgical treatment is needed for patients with pathological fracture and spinal cord compression. Most surgical procedures are curettage, internal fixation, and bone-filling to restore bone continuity and stability[8–11].

For bone filling, autogenous bone, tumor inactivated bone, allogeneic bone, and bone cement are clinically used [12,13]. Of these, bone cement is widely used due to its convenience, easy plastic filling, good biocompatibility, and suitable stiffness. However, its effect on myeloma cell viability has not been investigated. We have observed that use of polymethylmethacrylate (PMMA) bone cement as filler is associated with low rates of local recurrence [14].

Heat shock proteins (HSPs) play an important role in resistance multiple myeloma developing treatment [15]. 17-allylamine-17-demethoxyaminomycin (17-AAG), a derivative of the first generation gerdermycin inhibits heat shock protein 90 (HSP90) by blocking ATP conversion into ADP, resulting in the degradation of HSP-90's tumor-related substrates, hence suppressing tumor cell proliferation. 17-AAG is now in phase II and III clinical trials and is effective against various cancers, alone or in combination with other antineoplastic drugs. It exhibits high safety, a broad anticancer spectrum, and is not easily susceptible to resistance[16]. Its disadvantages include poor water solubility and obvious drug toxicity when used alone. The commonly used drug vehicles for 17-AAG (DMSO and nano-micelles) also have side effects, limiting its extensive use [17]. Wang et al found that combined rmhTRAIL and 17-AAG application in the treat multiple myeloma revealed enhance synergistic effects [18]. We used PMMA bone cement as carrier for 17-AAG, using the bone cement as a filler and as a sustained-release drug delivery system. This approach greatly reduced 17-AAG's unwanted side effects and increased local drug concentration. *In vitro* studies show that 17-AAG-loaded PMMA slowly releases 17-AAG, which induces MM apoptosis more strongly

than simple bone cement, confirming that drug-loaded bone cement strong inhibits myeloma *in vitro*. These findings offer rationale for developing anti-myeloma bone cement. Here, we further characterized this system *in vivo* using a mouse model.

The main surgical methods for treating MMBD are tumor curettage or resection, filling of bone defects, and internal fixation. The choice of bone fillers is determined by factors like plasticity, stiffness, and biocompatibility. Allogeneic bone and bone cement are the most commonly used. We previously found that in MMBD patients, PMMA bone cement is more effective in surgical bone filling [8]. Relative to simple bone cement, PMMA loaded with 17-AAG has a sustained apoptosis-promoting effect on myeloma cells [14]. However, this has not been verified *in vivo*. Here, we established a subcutaneous model of extramedullary plasmacytoma of myeloma in immunodeficient mice and investigated the anti-myeloma effect of PMMA and 17-AAG-PMMA as well as the underlying mechanism.

Methods

Preparation of PMMA and 17-AAG loaded PMMA bone cement column

Aseptic PMMA (5g) was evenly mixed with 2.5mL MMA liquid using a 20mL sterile syringe and rolled out on a sterile treatment towel at an average speed during the wire drawing period. Calipers and sterile blades were used to cut off at the length of 6mm, and 6 aseptic PMMA bone cement columns (18.85mm^3) made. 17-AAG (4.5mg) was dissolved in DMSO (0.25mL). The 18g/L reserve solution was prepared and stored away from light. Next, the PMMA bone cement (prepared as described above) was thoroughly mixed with the 18g/L reserve MMA liquid in a 20mL sterile syringe and rolled out on a sterile treatment towel at the average speed during the drawing period. Calipers and sterile blades were used to cut off at the length of 6mm, and 6 aseptic 17-AAG-PMMA bone cement columns (18.85mm^3) made.

Patient-derived xenograft mouse model generation

Multiple myeloma patient-derived xenograft mouse model were generated as previously described[19]. Briefly, myeloma fresh tumor tissues were obtained from patients who were diagnosed as extramedullary multiple myeloma(Supplemental Table 8). This study was approved by Beijing Chao-yang hospital institutional review board (IRB) (2018-ke-259), and all patients had written informed consent authorizing for the collection and use of tissues for study purposes. Fresh tumor tissue was divided into small pieces and subcutaneous inoculated into mice (Chinese Patent : 201810468838.1). Forty 6-week-old female NCG mice were transplanted with 10mm^3 tumor tissue. Tumor volume was measured twice a week by digital calipers. Then calculated tumor volume by the following formula: tumor volume =(major axis of tumor)×(minor axis of tumor) ^{2}/2. The mice were undergo surgery after tumor volumes reached 500mm^3.

Surgical intervention

Mice were anaesthetized by inhaling an anesthetic. Anesthetized mice were disinfected thrice at the tumor site using alcohol. The skin was then cut open with a scalpel blades along the tumor's long axis and a needle rotated about 1cm along the long axis of the tumor to expand the placement space for bone cement. Next, the bone cement column corresponding to each experimental group was inserted, with the control group receiving the same volume of 0.9% normal saline. After the cement column was fully inserted into the tumor, the puncture mouth was sutured with silk suture, and disinfected with alcohol. Upon regaining consciousness, the mice were returned to their corresponding cages. These experiments were carried out at 26℃ and 5% CO_2, in humidity.

Data collection

Tumors was measured twice a week. Tumor growth rate was given by tumor volume minus previous tumor volume, divided by the number of days between 2 measurements to get average daily tumor growth. Animal weight was monitored twice weekly on an electronic balance. Anal temperature was taken using a mouse electronic anal thermometer lubricated with paraffin oil, and then inserted 1cm into the rectum and temperature read after 1 min. Temperature was measured twice weekly.

Mouse endpoints and data measurement

After taking the general picture of the mice, the mice were sacrificed at the point of the experiment. The tumor was then completely removed and its cross section taken and the ratio between the tumor's necrotic area and sectional area calculated. The heart, liver, spleen, and kidneys were also collected and weighed. The tumor tissue was cut into 0.5-1cm^3 pieces and fixed in PFA overnight. Paraffin sections were prepared. They were then examined by HE staining and immunohistochemical staining. 12 visual fields were randomly selected in each group (magnification: 40X). Average optical density was evaluated on Image J.

Tannic acid staining

Two mice in each group were anesthetized. When anesthesia took effect, the chest cavity was opened immediately to expose the heart and the right atrial appendage cut through the ascending aorta of the left ventricle to open the right atrium. 40-80ml saline (37℃) was infused for rapid flushing. When the right atrial flow was better than the clear lavage fluid, the animals were immediately perfused with 150-200mL 2% PFA plus 2% tannic acid mixed mordant fixation solution. After 2 hours of fixation, the tumor on the back of the mouse was carefully excised with some tissue without destroying the capsule. Preparation of tumor slices, color was developed with 2% ferric chloride solution. Next, 10 visual fields were randomly imaged (40X magnification) in each group on an optical microscope and small arteries and veins (> 100μm), microarteries and veins (10–100μm) and capillaries (< 10μm) counted.

Vascular latex perfusion

One tumor-bearing mouse was anesthetized and the chest cavity opened to expose the heart. The ascending aorta was intubated and irrigated with warm saline (40–80 ml, 37℃) and the emulsion

perfused immediately after seeing excellent flow of the right atrium than the clear lavage fluid. After 24 h tissue fixation, the tumor was dissected and its blood supply examined.

Statistical analysis

SPSS 23.0 was used for all statistical analyses. One-way ANOVA was used to analyze tumor volume, growth rate, weight, organ weight, mouse weight, anal temperature, tumor necrosis area to tumor sectional area ratio, and average optical density of immunohistochemical staining. Log-rank test and Gehan-Breslow-Wilcoxon tests were used for mouse survival analysis. Nonparametric test was used to analyze tannic acid stained blood vessels. $P = < 0.05$ indicated statistically significant differences.

Results

17-AAG loaded PMMA bone cement inhibits tumor growth

All 18 NCG mice survived without postoperative bleeding, wound infection, or other complications. Initial tumor volumes in the control, PMMA, and 17-AAG-PMMA groups were 444.60±217.51mm^3, 480.23±161.40mm^3, and 442.68±139.63mm^3, respectively, and did not differ significantly. After surgical intervention (Figure 1), the tumor volume was measured twice weekly for 4 weeks (Supplement Table 1). This analysis revealed gradual growth in tumor volume over time (Figure 2A). Tumor growth was slow in all groups for first 3-6 days after operation, but accelerated thereafter. Beginning from the 1st week of the operation, tumor growth rate was highest in the control group, followed by the PMMA group, while the 17-AAG-PMMA group grew slowest. From the 10th day after operation, tumor growth rate in the control group was significantly higher than in the other 2 groups, while growth rate in the PMMA and 17-AAG-PMMA groups remained almost the same 1 week after the operation. There was difference between the control group and the PMMA group, and has significant difference between the control group and the 17-AAG-PMMA group.

The Kaplan-Meier survival curves of three groups of mice were generated (Figure 2B). This analysis found that mice in the 17-AAG-PMMA group prolonged than those in the PMMA group. Euthanasia performed when the tumor exceeds 2500mm^3. Log-rank test revealed statistically significant differences in survival rate among the control groups and 17-AAG-PMMA group, and there were not significant between other two groups.

17-AAG loaded PMMA bone cement affects tumor growth rate

From the 1st to 3rd day after operation, tumor growth rate in the control group was significantly higher than in the 17-AAG-PMMA group, but there was no significant difference between the control group and PMMA group. There was no significant difference in the tumor growth rate between 4-6 and 7-10 days after operation. From the 11th to 13th and 14th to 17th day after operation, tumor growth rate in control group was higher than in the PMMA and 17-AAG-PMMA group. There were no significant differences between the groups at 18-20 days after operation but at 21-24 days after operation, the tumor growth rate

in control group was significantly higher than in the simple bone cement and drug-loaded bone cement group. At 25-27 days after operation, there was no significant difference in tumor growth rate among the 3 groups (p>0.05, Supplement Table 2). Overall mean tumor growth rate analysis in the 3 groups found that tumor growth rate in the 17-AAG-PMMA and PMMA group was significantly slower relative to control group (p=<0.05, Figure 2C).

Comparison of tumor necrosis area

The intact tumor was cut perpendicularly along the long axis coronal plane (Figure 2D). The ratio of tumor section necrotic area to tumor section area was calculated on Image J and found to be 16.6±12.9%, 28.9±9.8% and 34.7±11.0%, in the control, PMMA, and 17-AAG-PMMA group respectively (Figure 2E). The ratio in the control group was significantly lower than in 17-AAG-PMMA group (p=<0.05). There was no significant difference between the control and PMMA group or PMMA and 17-AAG-PMMA group. HE staining revealed uniform mononuclear or multinucleated monoclonal plasma cells (dark purple), and more necrotic tissue around the bone cement (light pink), with the necrotic area largest in the 17-AAG-PMMA group, followed by PMMA group and smallest in the control group (Figure 2F).

17-AAG loaded PMMA bone cement reduced tumor angiogenesis.

Upon tannic acid staining and perfusion, the tumor was removed and the blood vessels observed. In the 3 groups (Figure 3A-C), vascular endothelial cells in the tumor stained grayish-black, and their branches, course, and distribution were clearly visible. Growth of tumor blood vessels is vigorous, and the distribution of blood vessels at all levels was irregular. Ten visual fields were randomly taken in each group on an optical microscope and counted small arteries and veins (>100μm), microarteries and veins (10-100μm), and capillaries (<10μm) (Supplement Table 3). The total number of blood vessels in control, PMMA, and 17-AAG-PMMA group was 96.80±7.22, 82.10±6.47, 42.40±8.15 respectively. The number of capillaries was 82.10±5.09, 73.10±7.33, and 38.00±7.29, respectively. The number of microarteries and veins was 12.70±4.00, 8±1.63, and 3.30±1.49, respectively. The number of small arteries and veins was 2±1.56, 1±1.05, and 1.10±1.19, respectively (Figure 3D-E). There were differences in the total number of blood vessels between control group and 17-AAG-PMMA group. There was no difference between control group and PMMA group. There were difference in the number of capillaries and microarteries between control group and 17-AAG-PMMA group.

17-AAG loaded PMMA bone cement promotes tumor apoptosis

Immunohistochemical staining revealed that Bax, Bcl-2, and active Caspase-3 are localized in the cytoplasm of myeloma cells (Figure 4A). In each group, 12 visual fields were randomly selected under a 40× objective lens (Figure 4B). Average optical density (AOD) of the positive areas in the visual field was calculated on image J (Supplement Table 4). Bax and active Caspase-3 expression in the 17-AAG-PMMA group was significantly higher than in controls, while Bcl-2 expression was significantly lower than in the control group. Active Caspase-3 expression in the PMMA group was significantly higher than in control group. While Bcl-2 expression was significantly lower relative to the control group. Bax expression did not

differ significantly between the 2 groups. Active Caspase-3 expression in 17-AAG-PMMA group was significantly higher than in the PMMA group but Bcl-2 expression in 17-AAG-PMMA group was significantly lower than in the PMMA group.

17-AAG loaded PMMA bone cement does not affect body weight and anal temperature in mice

Mouse body weight (Supplement Table 5) and anal temperature (Supplement Table 6) were measured twice weekly (Tuesday and Friday). Body weight of mice in the control, PMMA and 17-AAG-PMMA groups did not vary significantly (Figure 4C,). The mouse anal temperature was monitored (Figure 4D). There was no significant increase in anal temperature among the 3 groups, and there was no redness and swelling, no exudation, no suppuration.

17-AAG loaded PMMA bone cement does not affect organ weight

After the mice were sacrificed, we stripped mice heart, liver, spleen, lungs, bilateral kidneys, and brain. Use an electronic balance to weigh the internal organs. The weights of the heart, spleen, lung, kidney, and brain had no significantly difference between the PMMA and 17-AAG-PMMA group (Figure 4E, and Supplement Table 7)

Latex vascular perfusion

During tumor-bearing mice dissection, we observed that mouse axillary vessels sent out large branches from both sides of the head and tail of the tumor, which then enter the tumor from the periphery. These two vessels are the main blood suppliers to subcutaneous MM tumor in this model. In the branch vessels on the head side of the tumor, it was observed that a blood vessel enters the skin of the mouse's back. In the branch vessels on the caudal side of the tumor, no branch vessels were observed entering the skin, but several tertiary vessels originating from the trunk of the branch vessels were observed to enter the tumor (Figure 5A-D).

Discussion

Effect of 17-AAG loaded PMMA on tumor size, growth rate, and weight

In this study, difference in tumor growth rate across the 3 groups were noticed from the 3rd day after operation, with tumor growth fastest in the control group, followed by the PMMA group and then the 17-AAG-PMMA group. Indicating that PMMA and 17-AAG-PMMA significantly inhibit MM cells proliferation in mice and that the inhibitory effect of 17-AAG-PMMA was stronger. However, there was a point at which tumor growth rate in the control group was slower than that of the PMMA group, probably due to disruption of the tumor by the surgical intervention, thereby temporary slowing growth.

This study differs from other *in vivo* studies involving bone cement implantation into tumors [20]. In addition, the amount of bone cement in this experiment is too small, and the tumor volume increases over time. Thus, the anti-tumor effects of the bone cement weaken with time until finally, tumor weight differences are insignificant. Clinically, PMMA is often used to fill defects after tumor resection, which may inhibit the tumor more obviously, limiting MM's local recurrence. Because tumor weight is affected by many factors, it is not a reliable index for assessing the effectiveness of interventions.

To our knowledge, there are no reports on the application of drug-loaded bone cement or that bone cement affects cancer patient survival. Here, while log-rank tests in Kaplan-Meier survival analysis showed significant survival differences, results from Gehan-Breslow-Wilcoxon test did not show significant differences, indicating that drug-loaded bone cement could significantly improve long-term survival of NCG tumor-bearing mice, but not their short-term survival rate. This is consistent with past findings [21]. In this subcutaneous model of MM, tumor weight may influence mouse body weight. Tumor load reduction can significantly improve mouse survival. Whether changing the concentration and time of 17-AAG-PMMA positively affects patient survival is worthy of follow-up study.

Tumor necrotic area and distribution of tumor nutrient vessels

Differences in tumor volume may be due to tumor cell necrosis or apoptosis. Gross and HE staining showed that the necrotic area in the tumor tissue was centered on bone cement. The proportion of necrotic area in the drug-loaded bone cement group was significantly larger than in the control group but there was no significant difference between the simple bone cement group and the control group. Drug-loaded bone cement promoted significantly more tumor tissue necrosis. In addition to directly promoting apoptosis, interference with the tumor microenvironment may also inhibit tumor growth, whereby neovascularization is an important driver of myeloma proliferation. Renal function damage caused by angiography and was contraindicated for patients with MM. Studies on MM vessels mostly evaluate VEGF levels as an indirect index, but there is no method for directly visualizing tumor vessels.

To assess if differences in tumor blood vessel volume across the 3 groups is a reason for the differences in tumor necrosis area ratio, we for the first time used tannic acid-ferric chloride staining to visualize tumor blood vessels [22]. This staining method can specifically mordant vascular endothelium and morphologically distinguish between large, medium, and small vessels. This analysis found that the total number of blood vessels, capillaries and microarteries, and veins in the 17-AAG-PMMA group were significantly less than in the other 2 groups. Indicating that the drug-loaded bone cement affects tumor blood vessel number, enhancing tumor tissue necrosis. The effects and mechanism of 17-AAG and PMMA on vascular endothelial cells have not been previously studied and warrant further investigation.

Apoptosis mechanism of Multiple Myeloma cells

Apoptosis may occur via the mitochondrial, death receptor, or endoplasmic reticulum pathways. Bax and Bcl-2, Bcl-2 protein family members, are the most important regulators of apoptosis. By mediating the

release of cytochrome C into the cytoplasm via the mitochondrial pathway, they activate Caspase proteins, leading to apoptosis. While Bax promotes apoptosis, Bcl-2 inhibits apoptosis. Generally, the cellular levels of Bcl-2 and Bax proteins are relatively stable. Bcl-2 upregulation causes bax/bax homodimer dissociation in large quantities, which then associate with Bcl-2 into stable bcl-2/bax heterodimers, suppressing apoptosis induction and prolonging cell survival. Bax upregulation elevates bax/bax homodimer formation, promoting apoptosis [23,24].

The Caspase protein family has 14 members (caspase-1 to caspase-14) with various functions including enhancing pro-inflammatory cytokine maturation, apoptosis initiation, and apoptosis execution. Caspase-3 is the main downstream effector of apoptosis [25]. Activated Caspase-3 cleaves DNA-dependent protein kinase (DNA-PK) and Poly (ADP-ribose) polymerase (PARP), thereby modulating DNA replication, transcription, and damage repair. Here, we find that PMMA downregulates Bcl-2 and activated Caspase-3 levels, inducing MM apoptosis. The apoptosis-promoting effect of drug-loaded bone cement group is stronger than that of simple bone cement group, and it can also upregulate Bax protein, which is related to the apoptosis-promoting effect of 17-AAG on tumor cells. Past studies in other cancers show HSP90 inhibitors (including 17-AAG) upregulate Bax and downregulate Bcl-2, promoting apoptosis. 17-AAG-PMMA may directly induce MM cells apoptosis by upregulating expression of Bax, downregulating Bcl-2, and activating Caspase-3 [26,27]. Therefore, 17-AAG-PMMA has great potential in surgical treatment of MM.

Blood vessels that supply the tumor

Most studies on the tumor microenvironment have focused on the mechanisms of neovascularization (especially via VEGF) and microvessel density (MVD). However, as to where the tumor blood vessels come from, there is no evidence that the blood supply arteries within the tumor tissue are anastomosed with each other. Interventional embolization should make the embolic agent fill the tumor tissue as much as possible, and finally embolize the tumor feeding artery with gelatin sponge, which was confirmed by digital subtraction angiography (DSA) again after embolization [28].

Because multiple myeloma may be associated with renal function damage, angiography was disabled, so there is no study on the source of blood supply to the extramedullary plasmacytoma in multiple myeloma. Clinically, we have observed that extramedullary plasmacytoma of multiple myeloma has abundant blood supply and large amount of surgical bleeding. It is speculated that there may be large blood vessels, but it is not clear where such blood vessels come from, whether there are major blood vessels, whether they communicate with adjacent normal blood vessels, or how collateral circulation occurs. Here, we used latex perfusion to directly display the origin of mouse subcutaneous MM tumor vessels, which allowed the investigation of extramedullary plasmacytoma tumor vessels in MM. This analysis showed that the MM tumor was mainly supported by 2 blood vessels from the axillary vessels of the mice. We speculate that in patients with clinical MM extramedullary lesions, the extramedullary tumor should also be able to induce normal blood vessels to send out blood vessel branches to support the tumor tissue. According to this anatomical feature, in extramedullary MM tumors that are hard to directly

resect, it is necessary to find and block the feeding vessels so as to reduce blood supply to lesions or even to remove the lesions directly.

Biosafety analysis

In this study, there was no redness, swelling, or exudation of the skin after operation. No significant differences in anal temperature, body and organ weight, or rejection of PMMA or 17-AAG-PMMA were observed among the 3 groups, indicating that the amount of bone cement and the molar concentration of 17-AAG were tolerable in mice.

However, this study has some limitations. First of all, biologically, the tumors in the model are more similar to clinical extramedullary MM lesions. Due to a lack of interaction between human bone marrow and myeloma cells, MMBD is not fully reproducible. Moreover, we observed that tumor necrosis in the control group was significantly higher than in the other control group, which was not consistent with the clinical observation. Possibly because tumor volume of the subcutaneous model develops too fast, making it hard to sufficiently provide central blood supply to the tumor, leading to tissue necrosis. Secondly, to control the variables, only one patient's MM tumor tissue (IgA-κ type) was used, which may not represent all MM types. In future, it may be considered to join other MM organizations for a more comprehensive evaluation of the role of 17-AAG-PMMA bone cement. Finally, to unify the size and shape of the cement column, the polymerization heat production by PMMA bone cement was not included in this study. Therefore, in practice, the anti-tumor effect of PMMA bone cement and 17-AAG-PMMA may exceed the effects seen in our study.

Conclusions

17-AAG-loaded PMMA improved properties of PMMA, significantly enhancing its antitumor effects *in vivo*. This study can be applied to MMBD patients. However, other small molecules compounds may also be applied. This has profound implications for MMBD patients and indicates that interventions can be designed to improve antitumor effects.

Declarations

Compliance with ethical standards

Conflict of interest The author have declared no conflict of interest.

Funding

Natural Science Foundation of Beijing Municipality (7192071)

Ethical approval

This study was approved by Beijing Chao-yang hospital institutional review board (IRB)(2018-ke-259).

Informed consent

All patients had written informed consent authorizing for the collection and use of tissues for study purposes.

References

1. Rajkumar SV. Multiple myeloma: 2012 update on diagnosis, risk-stratification, and management. American journal of hematology. 2012;(87):78–88.
2. Alegre A, Gironella M, Bailén A, Giraldo P. Zoledronic acid in the management of bone disease as a consequence of multiple myeloma: a review. European journal of haematology. 2014; (92):181–188.
3. Kanellias N, Gavriatopoulou M, Terpos E, Dimopoulos MA. Management of multiple myeloma bone disease: impact of treatment on renal function. Expert review of hematology. 2018;(11):881–888.
4. Ring ES, Lawson MA, Snowden JA, Jolley I, Chantry AD. New agents in the Treatment of Myeloma Bone Disease. Calcified tissue international. 2018;(102): 196–209.
5. Vallet S, Filzmoser JM, Pecherstorfer M, Podar K. Myeloma Bone Disease: Update on Pathogenesis and Novel Treatment Strategies. Pharmaceutics. 2018(10):202.
6. Kelley SP, Ashford RU, Rao AS, Dickson RA. Primary bone tumours of the spine: a 42-year survey from the Leeds Regional Bone Tumour Registry. European spine journal: official publication of the European Spine Society, the European Spinal Deformity Society, and the European Section of the Cervical Spine Research Society. 2007;(16):405–409.
7. Hussein MA, Vrionis FD, Allison R, et al. The role of vertebral augmentation in multiple myeloma: International Myeloma Working Group Consensus Statement. Leukemia. 2008;(22):1479–1484.
8. Surgeon's Committee of the Chinese Myeloma Working Group of the International Myeloma Foundation. Consensus on Surgical Management of Myeloma Bone Disease. Orthopaedic surgery. 2016(8): 263–269.
9. Zadnik PL, Goodwin CR, Karami KJ, et al. Outcomes following surgical intervention for impending and gross instability caused by multiple myeloma in the spinal column. Journal of neurosurgery. 2015;Spine(22):301–9.
10. Denaro V, Denaro L, Albo E, Papapietro N, Piccioli A, Di Martino. Surgical management of spinal fractures and neurological involvement in patients with myeloma. Injury. 2016;47(Suppl 4):49-s53.
11. Igarashi K, Yamamoto N, Shirai Tet al. The long-term outcome following the use of frozen autograft treated with liquid nitrogen in the management of bone and soft-tissue sarcomas. The bone & joint journal.2014;(96-b): 555–561.
12. Kühn KD, Höntzsch D. Augmentation with PMMA cement. Der Unfallchirurg. 2015;(118):737–748.
13. Shen J, Du X, Zhao L, Luo H, Xu Z. Comparative analysis of the surgical treatment results for multiple myeloma bone disease of the spine and the long bone/soft tissue. Oncology letters. 2018; (15):10017–10025.

14. Usmani SZ, Bona R, Li Z. 17 AAG for HSP90 inhibition in cancer–from bench to bedside. Current molecular medicine. 2019;(9):654–664.
15. Grosicki S, Bednarczyk M, Janikowska G. Heat shock proteins as a new, promising target of multiple myeloma therapy. Expert review of hematology. 2020;(13):117–126.
16. Garcia-Carbonero R, Carnero A, Paz-Ares L. Inhibition of HSP90 molecular chaperones: moving into the clinic. The Lancet. Oncology. 2013;(14):e358-369.
17. Koto K, Murata H, Sawai Y, Ashihara E, Horii M, Kubo T. Cytotoxic effects of zoledronic acid-loaded hydroxyapatite and bone cement in malignant tumors. Oncology letters. 2017;(14):1648–1656.
18. Wang J, Li Y, Sun W, Liu J, Chen W. Synergistic effects of rmhTRAIL and 17-AAG on the proliferation and apoptosis of multiple myeloma cells. Hematology (Amsterdam, Netherlands). 2018;(23): 620–625.
19. Huang L, Okada K, Takahashi S, Suzuki N, Shimada Y, Itoi E. PDX-derived organoids model in vivo drug response and secrete biomarkers. JCI insight. 2020;(5): e135544.
20. Tani T, Hatanaka K, Watanabe H, Asano Y, Yamagata H, Maruyama T Doxorubicin-loaded calcium phosphate cement in the management of bone and soft tissue tumors. In vivo (Athens, Greece).2006; (20):55–60.
21. Matsui S, Doseff A, Chau BN, et al. A modification of Mayer's tannic acid-ferric chloride staining method for demonstrating cellular membranous systems for light microscopy. Biotechnic & histochemistry: official publication of the Biological Stain Commission. 2000;(75):33–40.
22. Kirsch DG, Yamamoto S, Win TT. Shwe. et al. Caspase-3-dependent cleavage of Bcl-2 promotes release of cytochrome c. The Journal of biological chemistry. 1999;(274): 21155–21161.
23. Tsukahara S, et al. Inhalation of low-level formaldehyde increases the Bcl-2/Bax expression ratio in the hippocampus of immunologically sensitized mice. Neuroimmunomodulation. 2006;(13):63–68.
24. Odonkor CA, Achilefu S. Modulation of effector caspase cleavage determines response of breast and lung tumor cell lines to chemotherapy. Cancer investigation. 2009;27:417–29. doi:10.1080/07357900802438585.
25. Calero R, Morchon E, Martinez-Argudo I, Serrano R. Synergistic anti-tumor effect of 17AAG with the PI3K/mTOR inhibitor NVP-BEZ235 on human melanoma. Cancer letters. 2017;(406):1–11.
26. Tavernier E, et al. HSP90 inhibition results in apoptosis of Philadelphia acute lymphoblastic leukaemia cells: an attractive prospect of new targeted agents. Journal of cancer research and clinical oncology.2012;(138):1753–1758.
27. Zhang X, Gao F, Zhong S. Combinatorial Inhibition of mTORC2 and Hsp90 Leads to a Distinctly Effective Therapeutic Strategy in Malignant Pheochromocytoma. Current cancer drug targets. 2019; (19): 698–706.
28. Yata K, Yaccoby S. The SCID-rab model: a novel in vivo system for primary human myeloma demonstrating growth of CD138-expressing malignant cells. Leukemia. 2004;(18): 1891–1897.

Figures

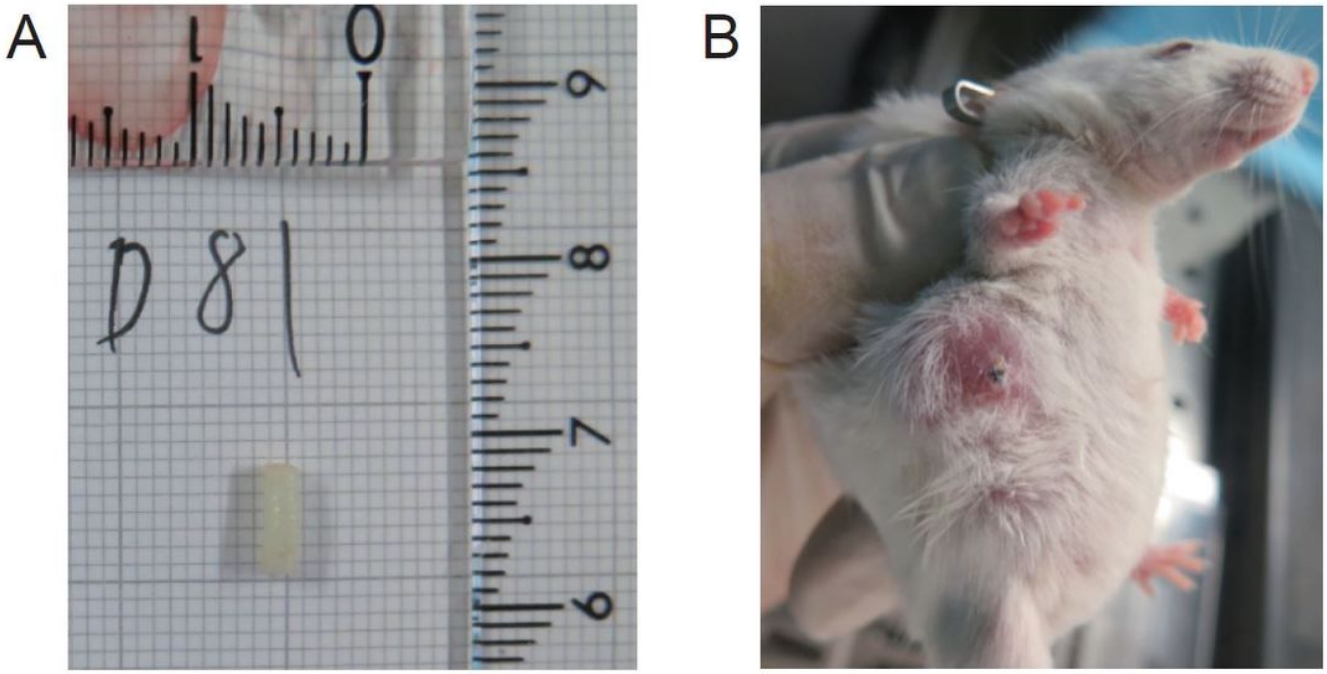

Figure 1

Surgical operation on mice. A. Images of the bioactive PMMA bone cement prepared for surgery. B. An image of mouse after implantation of PMMA bone cement.

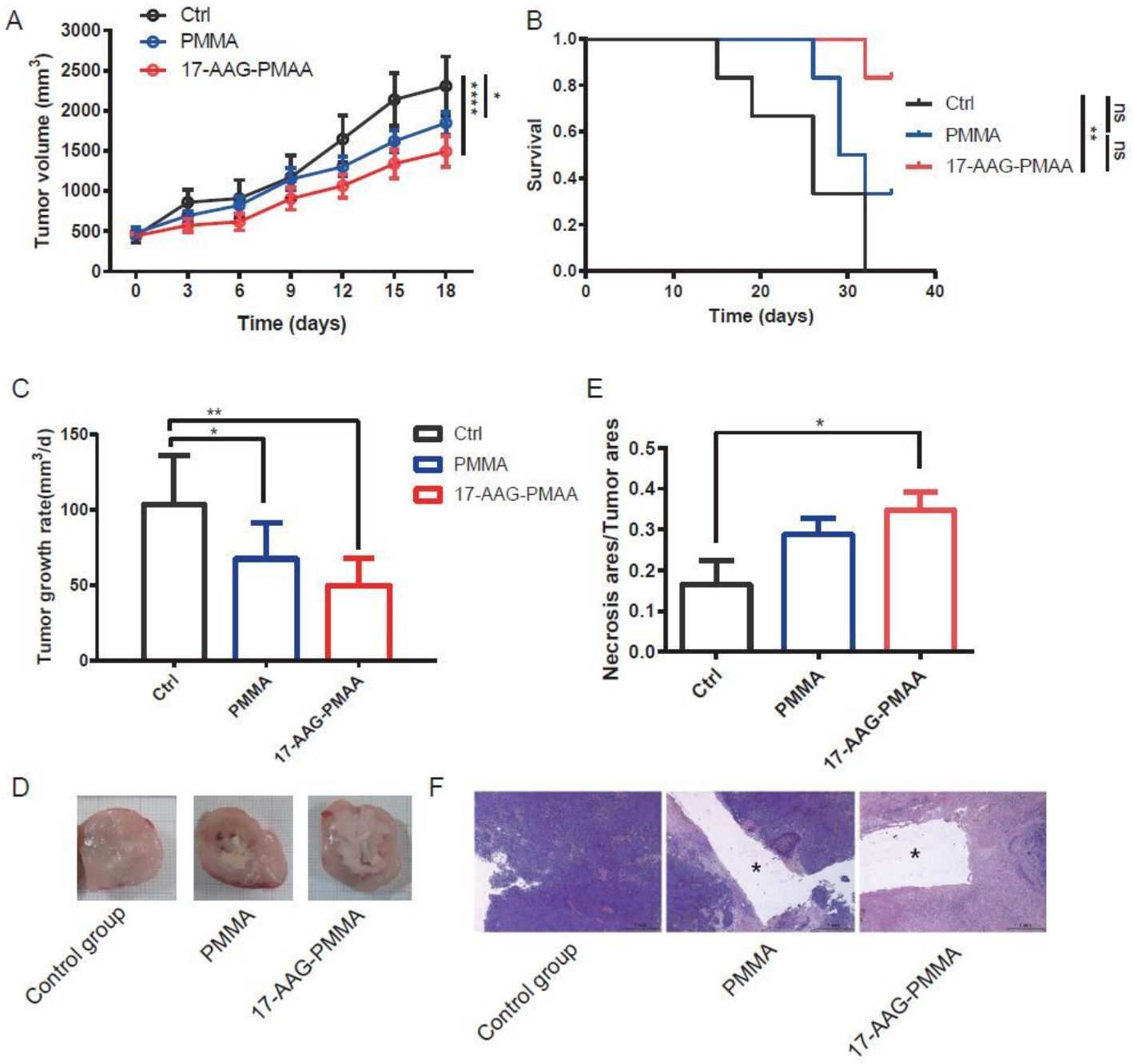

Figure 2

17-AAG-loaded polymethyl methacrylate bone cement suppressed tumor development in PDX-model. A. Tumor growth curves of patient multiple myeloma tumor tissue in NCG mice. B. Kaplan-Meier survival plot for mice. C. Tumor growth rate of tumor tissue from patients with multiple myeloma in NCG mice. D. Representative diagram of tumor growth rate in (C). E. Anatomical map of the tumor tissue from patients with multiple myeloma in NCG mice. F. Representative diagram of necrotic rate in (E). Tumor volumes were compared using two-way ANOVA, and survival data were analyzed using a log-rank (Mantel-Cox) test. Data were analyzed using two-tailed unpaired t tests (D, F); *p < 0.05, **p < 0.01, ***p < 0.001, ****p < 0.0001. All error bars denote SEM.

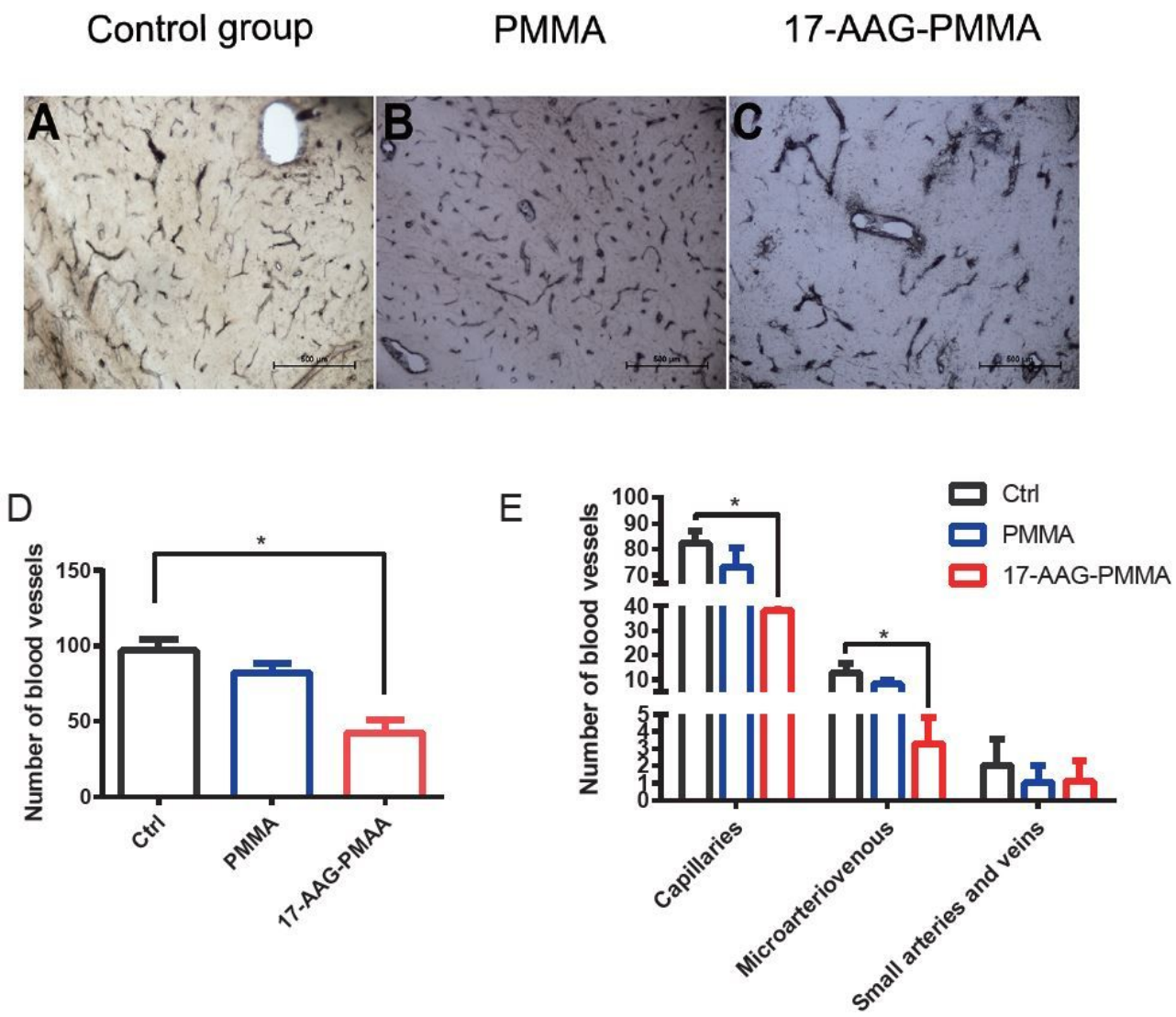

Figure 3

17-AAG-loaded polymethyl methacrylate bone cement reduced angiogenesis in PDX-model. Tumor angiogenesis in control group (A), PMMA group (B), 17-AAG-PMMA group (C). D. A representative diagram of tumor angiogenesis. E. Morphological features of blood vessels. Data were analyzed using two-tailed unpaired t tests (D, E); *p < 0.05. All error bars denote SEM.

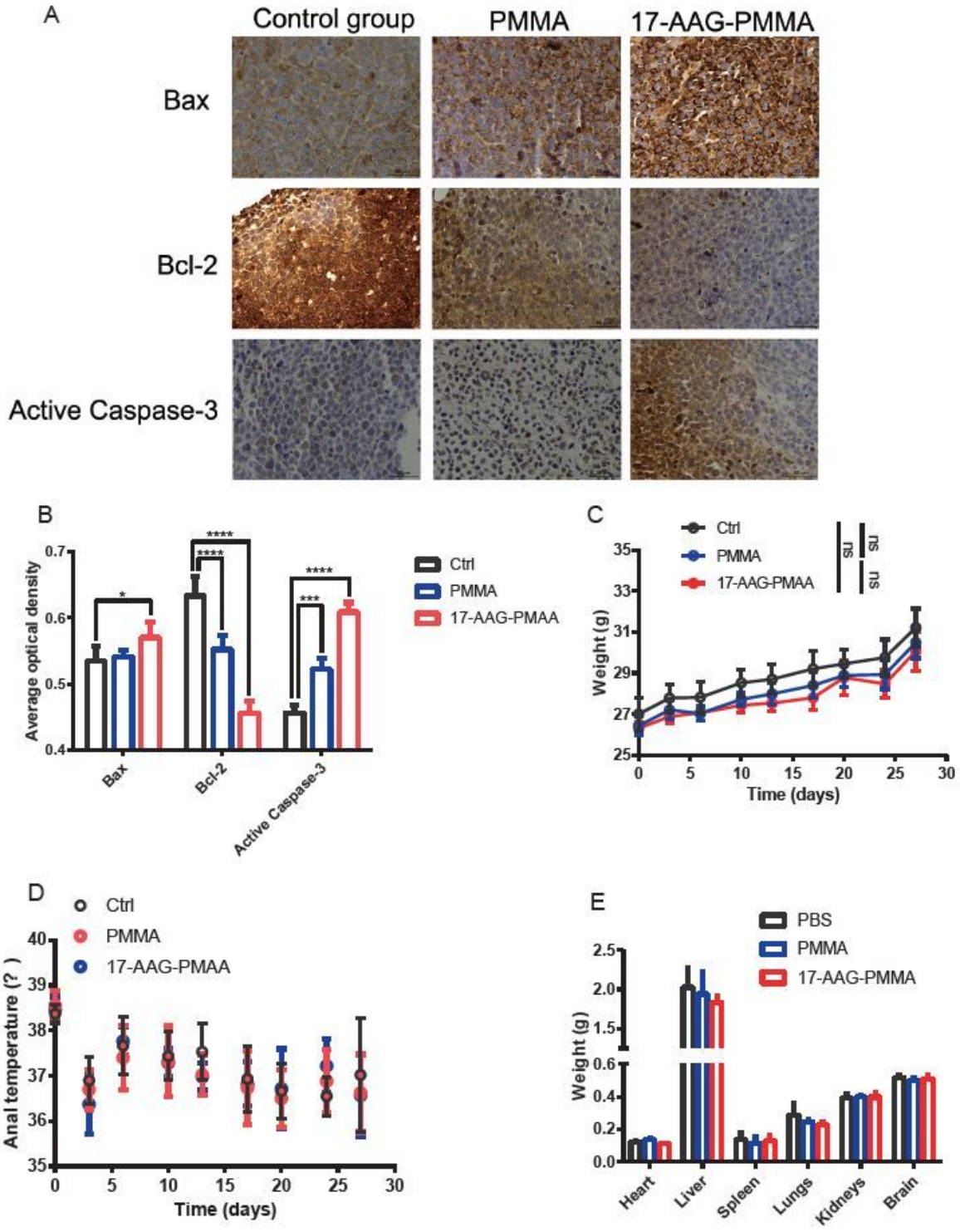

Figure 4

17-AAG-loaded polymethyl methacrylate bone cement promoted apoptosis of tumor cells but did not affect the body weight, anal temperature and organ weight. A. IHC results showing expression of Bax, Bcl-2, and active Caspase-3. B. Representative diagram of average optical density in (A). C. Body weight curve of different days. D. Anal temperature measured in different days. E. Organ weight of PDX-model in

vivo. Data were analyzed using two-tailed unpaired t tests (B); *p < 0.05, ** p < 0.01, ***p < 0.001, ****p < 0.0001. All error bars denote SEM.

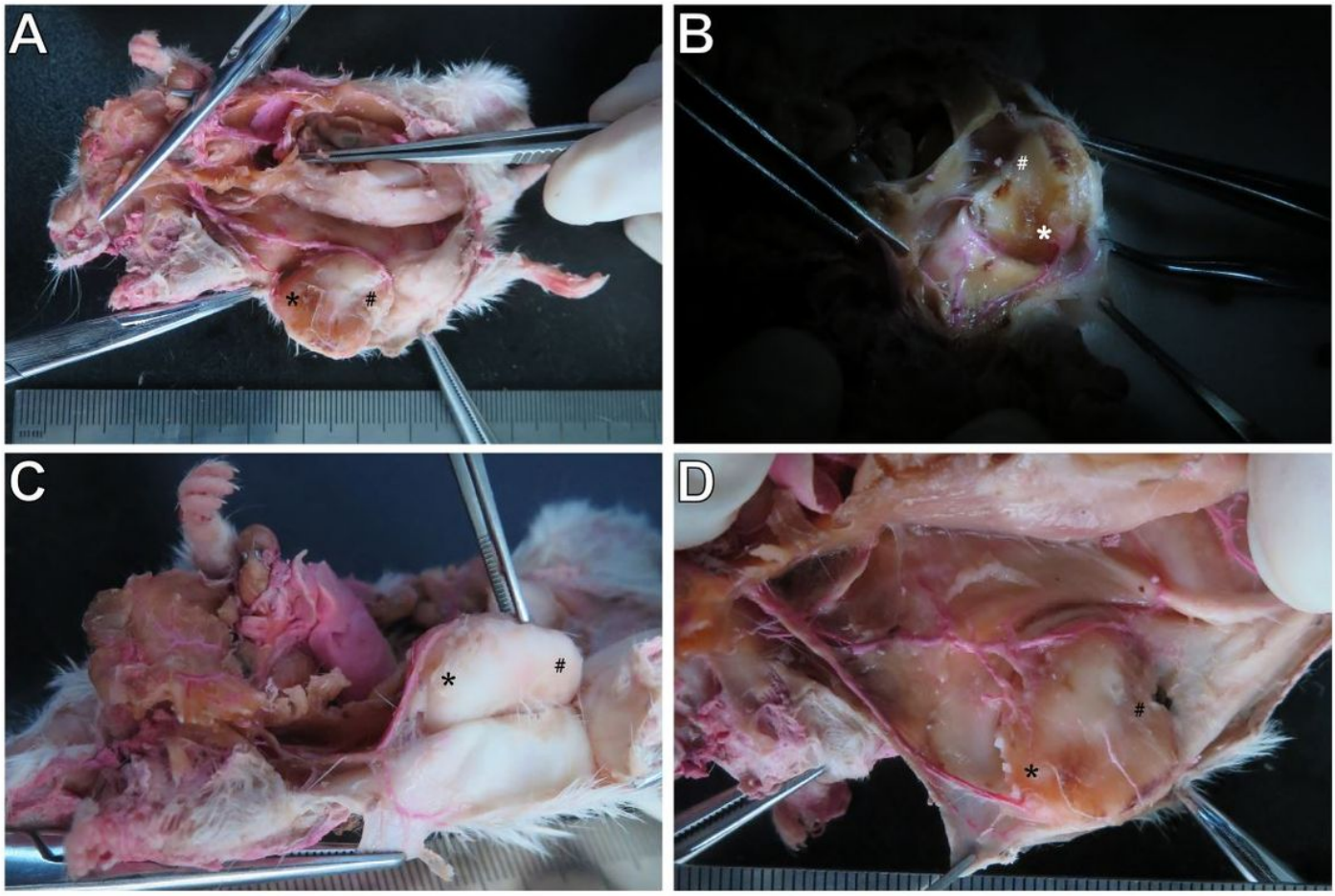

Figure 5

Image of tumor blood vessels after latex perfusion in mice. A, B, C, D represents different mice. * represents the side of tumor head, # represents the side of tumor caudal.

Supplementary Files

This is a list of supplementary files associated with this preprint. Click to download.

- supplementarytable17.docx
- supplementarytable8.docx